Micromechanics-Based Interfacial Debonding Model of Functionally Graded Materials

G. H. Paulino[a], H. M. Yin[a], and L. Z. Sun[b]

[a]*Department of Civil and Environmental Engineering*
University of Illinois at Urbana-Champaign, Urbana, IL 61801
[b]*Department of Civil and Environmental Engineering*
University of California, Irvine, CA 92697

Abstract. This study develops a micromechanical damage model for two-phase functionally graded materials considering the interfacial debonding of particles and pair-wise interactions between particles. Given an applied mechanical loading, in the particle-matrix zones, the interactions from all other particles over the representative volume element are integrated to calculate the homogenized elastic fields. The progressive damage process is dependent on the applied loading and is represented by the debonding angles which are obtained from the relation between the particle stress and the interfacial strength. In terms of the elastic equivalency, the debonded, isotropic particles are replaced by the perfectly bonded, orthotropic particles. The effective elasticity distribution in the gradation direction is correspondingly solved. Numerical simulations are implemented to illustrate the capability of the proposed model.

Keywords: Functionally graded composites; Micromechanical modeling; Effective elasticity; Damage mechanics; Interfacial debonding.

INTRODUCTION

Since the mechanical behavior of functionally graded materials (FGMs) depends on microstructures including the heterogeneous constituents, their deformation and damage failure mechanisms are different from each of the monolithic constituents. One of the predominant damage mechanisms is the interfacial debonding between the particles and the matrix [1]. Prader and Degisher [2] observed particle debonding when the composites were subjected to an external loading. In Figure 1, a particle is initially perfectly bonded to a continuous matrix [Figure 1(a)]. When the normal interfacial stress exceeds the interfacial strength due to the external loading in the direction, the particle starts to debond from the matrix [Figure 1(b)]. Then, the interfacial stress relaxes and the interfacial debonding may be stabilized. Thus, the damage results in the reduction in the effective stiffness of the overall material. Several investigations of the interfacial debonding in homogeneous composites have been proposed in the literature [3-6]. However, the effects of the interfacial debonding on the effective behavior of FGMs have not been addressed yet.

Due to the graded microstructure, the local field in FGMs not only greatly changes between two phases, but also spatially varies in the gradation direction. Thus, the interfacial debonding may only occur in some specific particles, and the magnitude of the damage also spatially depends on the location in the gradation direction. The

CP973, *Multiscale and Functionally Graded Materials 2006*
edited by G. H. Paulino, M.-J. Pindera, R. H. Dodds, Jr., F. A. Rochinha, E. V. Dave, and L. Chen

debonding further changes the local field through particle interactions, so the damage evolution is fully coupled with the mechanical response in the gradation direction. Therefore, the interfacial debonding of particles provides a significant effect on both the local fields in the microscopic scale and effective material properties in the macroscopic scale.

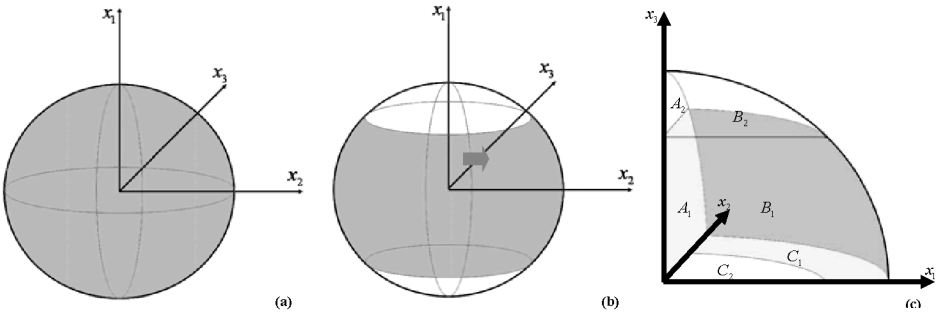

FIGURE 1. Schematic illustration for interfacial debonding of a spherical particle embedded in continuous matrix: (a) initially the particle perfectly bonded to the matrix, (b) the particle partially debonded from the matrix in the x_3 direction, and (c) projections of the debonded area.

This paper is the very first step toward investigating damage of functionally graded particulate materials by means of a multiscale approach based on micromechanics principles. Essentially, it combines the techniques of Yin et al. [7] and Liu et al. [6]. Although this preliminary investigation has several limitations, it offers a promising approach with room for further improvements.

FORMULATION

Consider an FGM containing two phases A and B with isotropic elastic stiffness $\mathbf{C}^A$ and $\mathbf{C}^B$, respectively. The global coordinate system of the FGM is denoted by (X_1, X_2, X_3) with X_3 being the continuous gradation direction. The overall grading thickness of the FGM is t. Three material zones exist in the gradation direction: Zone I ($0 \le X_3 \le d_1$) including phase A particles with phase B matrix, the Zone III ($d_2 \le X_3 \le t$) including phase B particles with phase A matrix, and the transition Zone II ($d_1 \le X_3 \le d_2$). When the FGM is subjected to a uniform far-field stress $\boldsymbol{\sigma}^0$ applied on the X_3 boundary, the averaged stress in each $X_1 - X_2$ layer should be the same as $\boldsymbol{\sigma}^0$, based on the equilibrium condition. The averaged stress and strain in the $X_1 - X_2$ layer are defined as the volume average of the stress and strain on the two phases, and are expressed as

$$\boldsymbol{\sigma}^0 = \phi(X_3)\mathbf{C}^A : \langle \boldsymbol{\varepsilon} \rangle^A (X_3) + \left[1 - \phi(X_3)\right]\mathbf{C}^B : \langle \boldsymbol{\varepsilon} \rangle^B (X_3), \tag{1}$$

$$\langle \boldsymbol{\varepsilon} \rangle (X_3) = \phi(X_3)\langle \boldsymbol{\varepsilon} \rangle^A (X_3) + \left[1 - \phi(X_3)\right]\langle \boldsymbol{\varepsilon} \rangle^B (X_3). \tag{2}$$

Using Yin et al. [7], we can obtain the averaged particle strain in terms of the arbitrary material point X_3

$$\begin{aligned}\langle\boldsymbol{\varepsilon}\rangle^{A}(X_3) = (\mathbf{I}-\mathbf{P}_0\cdot\Delta\mathbf{C})^{-1}:\langle\boldsymbol{\varepsilon}\rangle^{B}(X_3)+\phi(X_3)\Delta\mathbf{C}^{-1}\cdot\mathbf{D}(X_3):\langle\boldsymbol{\varepsilon}\rangle^{B}(X_3)\\ +\phi_{,3}(X_3)\Delta\mathbf{C}^{-1}\cdot\mathbf{F}(X_3):\langle\boldsymbol{\varepsilon}\rangle^{B}_{,3}(X_3)\end{aligned}, \quad (3)$$

where $(\mathrm{P}_0)_{ijkl}=[\delta_{ij}\delta_{kl}-(4-5\nu_0)(\delta_{ik}\delta_{jl}+\delta_{il}\delta_{jk})/[30\mu_0(1-\nu_0)]$, $\Delta\mathbf{C}=\mathbf{C}_1-\mathbf{C}_0$, and $\mathbf{D}$ and $\mathbf{F}$ represent the contributions of interactions from all other particles. Their explicit forms can be found in Yin et al. [7].

In the particle-matrix zone with $0\le X_3\le d_1$, the boundary at $X_3=0$ corresponds to the 100% matrix material (i.e., $\phi(0)=0$). The corresponding boundary conditions can be proposed as

$$\langle\boldsymbol{\varepsilon}\rangle^{B}(0)=\mathbf{C}^{B^{-1}}:\boldsymbol{\sigma}^{0}. \quad (4)$$

With the combination of Eqs. (1), (3), and (4), the averaged strain tensors in both phases can be numerically solved on the basis of standard backward Eulerian method. Similarly, in the other particle-matrix with the range of $d_2\le X_3\le t$ (zone III), we can also calculate the averaged strain fields by the switch of matrix and particle phases.

For the transition zone II ($d_1<X_3<d_2$), a phenomenological transition function [7] is introduced as

$$f(X_3)=\left[1-2\frac{\phi(X_3)-\phi(d_1)}{\phi(d_1)-\phi(d_2)}\right]\left[\frac{\phi(X_3)-\phi(d_2)}{\phi(d_1)-\phi(d_2)}\right]^2, \quad (5)$$

so that the averaged strain of each phase (A or B) in the transition zone II can be approximated as a cubic Hermite function appropriately contributed by the averaged strain of the same phase (A or B) from two particle-matrix zones (zones I and III). Namely,

$$\langle\boldsymbol{\varepsilon}\rangle^{A\text{ or }B}_{zone-II}(X_3)=f(X_3)\langle\boldsymbol{\varepsilon}\rangle^{A\text{ or }B}_{zone-I}(X_3)+\left[1-f(X_3)\right]\langle\boldsymbol{\varepsilon}\rangle^{A\text{ or }B}_{zone-III}(X_3). \quad (6)$$

The overall averaged strain tensor at each layer in the transition zone can be further obtained from Eq. (2). However, because the microstructure of the transition zone is not truly characterized, this treatment only provides a phenomenological approximation for the averaged strain in the transition instead of a rigorous solution.

When the applied loading $\boldsymbol{\sigma}^0$ is small, the particles are perfectly bonded to the matrix. However, with increase of applied load, the interfacial normal stress can reach the interfacial debonding strength so that particles start to debond from the matrix. The stress on the debonded surface area is released with extra deformation allowed. Thus, the effective stiffness of the particles reduces as a result of the increase of debonding area. In the present damage model, when partial interfacial debonding occurs, the equivalent stiffness method [6] is introduced; i.e., the partially debonded isotropic particles are replaced by fictitious orthotropic yet perfectly bonded particles. Consequently, the above micromechanical analysis is still applicable.

For simplicity, the averaged stress of particles is assumed to represent the interfacial stress so that the interfacial normal stress is expressed as

$$\sigma^{normal} = \mathbf{t}^T \cdot \bar{\boldsymbol{\sigma}} \cdot \mathbf{t} . \tag{7}$$

where $\mathbf{t}$ is the outward normal vector at any point at the interface. By comparing the interfacial normal stress with the interfacial debonding strength σ_{cri} at any surface point, we can solve the debonding area on the surface of the particle as a function of debonding angles to the directions of the three principal stresses $(\sigma_1, \sigma_2, \sigma_3)$ in the particles. Initially, the loading is small so that all the principal stresses are less than the interfacial strength. With further increase of the far-field loading, following Liu et al. [6] for composite materials, the interfacial debonding spreads in the following three categories. In each category, for one-eighth of a particle with structural symmetry, the debonding area is described by two debonding angles, which are defined in terms of the principal stresses and the interfacial strength and vary in the range of 0 to $\pi/2$ [6]. Three damage parameters D_i $(i = 1, 2, 3)$, projections of the debonding area in three principal directions normalized by the total projected area, are derived to evaluate the loss of the particles' tensile load-transfer capacity for each category as:

Category 1 $\sigma_1 \geq \sigma_{cri} \geq \sigma_2 \geq \sigma_3$

Only the first principal stress is greater than the interfacial strength σ_{cri}. The interfacial debonding initiates from the first principal direction, which is corresponding to the white area on the surface of the particle in Figure 1(b), and propagates towards the other two principal directions. Figure 1(c) shows one eighth of the debonded particle. Here, A_2, B_2, and C_2 denote the projections of the debonded area onto the three mid-planes of $x_2 - x_3$, $x_3 - x_1$, and $x_1 - x_2$, respectively; and A_1, B_1, and C_1 denote the corresponding projections of the undebonded area. Therefore, $A_1 + A_2 = B_1 + B_2 = C_1 + C_2 = \pi a^2 / 4$. The three damage parameters are expressed as

$$\begin{aligned}
D_1 &= \frac{A_2}{\pi a^2/4} = \frac{\sigma_1 - \sigma_{cri}}{\sqrt{(\sigma_1 - \sigma_2)(\sigma_1 - \sigma_3)}} \\
D_2 &= \frac{B_2}{\pi a^2/4} = \frac{2}{\pi}\left(\arcsin\sqrt{\frac{\sigma_1 - \sigma_{cri}}{\sigma_1 - \sigma_3}} - \sqrt{\frac{\sigma_1 - \sigma_{cri}}{\sigma_1 - \sigma_3}}\sqrt{\frac{\sigma_{cri} - \sigma_2}{\sigma_1 - \sigma_2}} \right). \\
D_3 &= \frac{C_2}{\pi a^2/4} = \frac{2}{\pi}\left(\arcsin\sqrt{\frac{\sigma_1 - \sigma_{cri}}{\sigma_1 - \sigma_2}} - \sqrt{\frac{\sigma_1 - \sigma_{cri}}{\sigma_1 - \sigma_2}}\sqrt{\frac{\sigma_{cri} - \sigma_3}{\sigma_1 - \sigma_3}} \right)
\end{aligned} \tag{8}$$

Category 2 $\sigma_1 \geq \sigma_2 \geq \sigma_{cri} \geq \sigma_3$

Two principal stresses are greater than the interfacial strength σ_{cri}. The interfacial debonding propagates around the particle, which is corresponding to the gray area on the surface of the particle in Figure 1(b), but still bond to the matrix along two ends in the other principal direction. In Figure 1(c), A_1, B_1, and C_1 denote the projections of the debonded area onto the three mid-planes of $x_2 - x_3$, $x_3 - x_1$, and $x_1 - x_2$, respectively. As a result, the three damage parameters are obtain as

$$D_1 = \frac{B_1}{\pi a^2/4} = \frac{2}{\pi}\left(\arcsin\sqrt{\frac{\sigma_2-\sigma_{cri}}{\sigma_2-\sigma_3}} + \sqrt{\frac{(\sigma_1-\sigma_{cri})(\sigma_{cri}-\sigma_3)}{(\sigma_1-\sigma_3)(\sigma_2-\sigma_3)}}\right)$$

$$D_2 = \frac{C_1}{\pi a^2/4} = \frac{2}{\pi}\left(\arcsin\sqrt{\frac{\sigma_1-\sigma_{cri}}{\sigma_1-\sigma_3}} + \sqrt{\frac{(\sigma_2-\sigma_{cri})(\sigma_{cri}-\sigma_3)}{(\sigma_1-\sigma_3)(\sigma_2-\sigma_3)}}\right). \tag{9}$$

$$D_3 = \frac{A_1}{\pi a^2/4} = 1 - \frac{\sigma_{cri}-\sigma_3}{\sqrt{(\sigma_1-\sigma_3)(\sigma_2-\sigma_3)}}$$

Category 3 $\sigma_1 \geq \sigma_2 \geq \sigma_3 \geq \sigma_{cri}$

In this case, all principal stresses exceed the interfacial strength. Thus, the entire interface is debonded as a void and the particle cannot transfer any tensile loading. The damage parameters are written as

$$D_1 = D_2 = D_3 = 1. \tag{10}$$

With the increase of the damage of particles, a larger deformation is permitted and thus the overall composite becomes more compliant. To simulate the stiffness softening, the damaged particle is replaced by the fully bonded one, but with reduced stiffness in certain directions corresponding to the damage parameters. Thus, the anisotropic, equivalent stiffness tensor of the damaged particle reads:

$$\tilde{C}_{ijkl}^{A \text{ or } B} = \lambda_{IK}^{A \text{ or } B}\delta_{ij}\delta_{kl} + \mu_{IJ}^{A \text{ or } B}\left(\delta_{ik}\delta_{jl} + \delta_{il}\delta_{jk}\right), \tag{11}$$

where the two second-rank tensors related to damage parameters are

$$\lambda_{IK}^{A \text{ or } B} = \lambda^{A \text{ or } B}(1-D_I)(1-D_K), \quad \mu_{IJ}^{A \text{ or } B} = \mu^{A \text{ or } B}(1-D_I)(1-D_J). \tag{12}$$

with the particle as either phase A or phase B.

To test the effective elasticity at any loading condition, an extra infinitesimal testing stress is applied on the lower and upper FGM boundaries, and then the averaged strain distribution in the gradation direction is calculated from the above formulation. From the relation between the testing stress and the increment of the averaged strain, we calculate the effective elasticity distribution. For instance, given a small uniaxial testing loading $\Delta\sigma_{33}$ on the lower and upper FGM boundaries, we solve the increment of the averaged strain as $\Delta\varepsilon(X_3)$. Then, the effective Young's modulus and the Poisson's ratio at any material layer can be derived as:

$$E(X_3) = \frac{\Delta\sigma_{33}}{\Delta\varepsilon_{33}(X_3)}; \quad v(X_3) = -\frac{\Delta\varepsilon_{11}(X_3)}{\Delta\varepsilon_{33}(X_3)}. \tag{13}$$

RESULTS AND DISCUSSION

To demonstrate the capability of the proposed model, two loading types are illustrated: uniaxial loading and shear loading, which correspond to FGMs subjected to negative pressure and frictional loading, respectively, in their applications. The sample FGM is the C/SiC FGM with the silicon carbide as phase A ($E_A = 320GPa, v_A = 0.3$) and the carbon as phase B ($E_B = 28GPa, v_B = 0.3$). The

interfacial debonding strength is assumed as $\sigma_{cri} = 100MPa$ .The lower and upper bounds d_1 and d_2 are selected where the corresponding volume fractions are 40% and 60%, respectively. The volume fraction distribution is assumed to be linear.

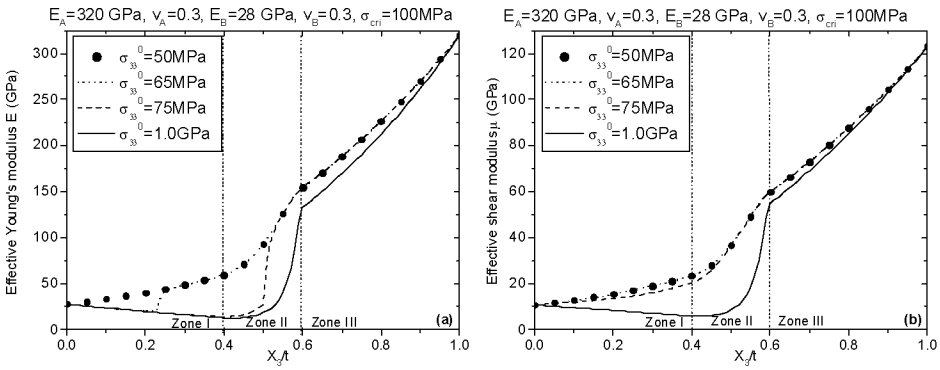

FIGURE 2. Results for the uniaxial tensile loading: (a) effective Young's modulus distribution; and (b) effective shear modulus distribution.

Figures 2(a) and 2(b) demonstrate the elastic modulus distributions in the gradation direction changing with the uniaxial tensile loading. For $\sigma_{33}^0 = 65MPa$, particles debond in the range of $0 \le X_3 \le 0.24t$ in the zone I, and in this range the effective Young's modulus decreases along with the value of X_3 and rapidly increases to the value for $\sigma_{33}^0 = 50MPa$ at $X_3 = 0.24t$ due to no debonding; whereas the effective shear modulus still increase and is almost the same as that for $\sigma_{33}^0 = 50MPa$. The above observation is due to the fact that the debonding angles are small and the debonding area is along two caps of particles in the loading direction, having a larger projection in the loading direction but much smaller projections in the other two directions. Thus the effective Young's modulus is reduced much faster than the shear modulus comparing with those for the fully bonded condition. For $\sigma_{33}^0 = 75MPa$, the debonding range in the FGM becomes larger as $0 \le X_3 \le 0.51t$ and the debonding angles also increase comparing with those for $\sigma_{33}^0 = 65MPa$.

REFERENCES

1. S. Suresh, A. Mortensen and A. Needleman, Fundamentals of Metal-Matrix Composites. Butterworth-Heinemann Publisher, Boston, 1993.
2. P. Prader and P. Degisher, Proc. 12th Internat. Conf. Compos. Mater., ICCM12, Paris, 1999.
3. I. Jasiuk and Y. Tong, In: Reddy, J.N. and Teply, J.L. (eds), Proc. 3rd Joint ASCE/ASME Mech. Conf., pp. 49–54, 1989.
4. J. Qu, *Mech. Mater.*, **14,** 269–281(1993).
5. L. Z. Sun, J. W. Ju and H. T. Liu, *Mech. Mater.*, **35**, 559–569 (2003).
6. H. T. Liu, L. Z. Sun, and J. W. Ju, *Inter. J. Damage Mech.*, **13**, 163-185 (2004).
7. H. M. Yin, L. Z. Sun and G. H. Paulino, *Acta Mater.*, **52**, 3535-3543 (2004).